White Rose
university consortium
Universities of Leeds, Sheffield & York

eprints@whiterose.ac.uk
https://eprints.whiterose.ac.uk/

Spinning Beta Silks Requires Both pH Activation and Extensional Stress

Andreas Koeppel, Nicola Stehling, Cornelia Rodenburg, and Chris Holland*

Synthetic silk production has undergone significant technological and commercial advances over the past 5 years, with fibers from most labs and companies now regularly matching the properties of natural silk by one metric or another. Yet the fundamental links between silk protein processing and performance remain largely unresolved and fiber optimization is commonly achieved through non-natural methods. In an effort to address this challenge, data that closes this loop of processing and performance is presented by spinning a native silk feedstock ex vivo into a near-native fiber using just two naturally occurring parameters; pH activation and extensional flow (i.e., spinning rate). This allows us to link previous experimental and modelling hypothesis surrounding silk's pH responsiveness directly to multiscale hierarchical structure development during spinning. Finally, fibers that match, and then exceed, natural silk's mechanical properties are spun and understood by rate of work input. This approach not only provides energetic insights into natural silk spinning and controlled protein denaturation, but is believed will help interpret and improve synthetic silk processing. Ultimately, it is hoped that these results will contribute towards novel bioinspired energy-efficient processing strategies that are driven by work input optimization and where excellent mechanical properties are self-emergent.

1. Introduction

Natural silk-spinning combines benign processing with outstanding mechanical performance, offering a means to create synthetic (bio)polymer materials with minimal energy input.[1] Serving as inspiration, silk's desirable properties are a direct result of a multi-scale hierarchical structure carefully developed during spinning.[2,3] However, efforts to replicate this process have historically fallen short due to a reliance on unnatural feedstocks, processing methods, and the wide range of process variables encountered. In addition, such efforts are yet to include a quantitative discussion of process energy efficiency, a topic becoming increasingly important from both an industrial and consumer perspective.[4,5]

When using the natural system as a biological blueprint, it is both necessary and important to look at the process variables involved in natural fiber formation. It is well established that during natural spinning, aqueous silk proteins experience chemical changes (ions,[6–9] pH[10,11]) and mechanical stress (shear, extensional[12]). However, the specific contributions of each variable towards natural fiber formation are only just beginning to be determined as previously they have been investigated in isolation or their in vivo importance is assumed through the perspective of artificial spinning systems.[13–17] We believe this disconnect requires more attention as, without this understanding, one cannot claim that any artificial spinning process is truly biomimetic.

For natural spinning the current consensus is that shifts in the chemical environment in the silk gland serve to control silk protein hydration and interaction, making them more or less susceptible to denature and aggregate as a result of an applied flow field.[3,4,18–20] For example, it has been shown by our group that the monovalent/divalent metal ion ratio is correlated with viscosity in the silk gland and influences protein alignment and aggregation under flow;[21,22] potentially providing optimized storage conditions[8] and mediating interactions between charged side groups during spinning.[7,23] This hypothesis has been recently validated through the direct introduction of metal ions into native silk feedstocks and a rheological model based on sticky reptation.[24]

However, a far greater body of evidence surrounds the influence of pH during spinning. Numerous studies have observed a consistent drop in pH along the gland and duct.[3,19] This, combined with reports of pH inducing changes in silk protein conformation[6,16,17,20,23,25,26] and rheological properties[27] strongly suggest that pH is also used to control silk protein stability and interactions. Specifically, small changes in pH have been shown experimentally to cause native silk proteins to refold[23] and through simulation and recombinant systems this phenomenon has been attributed to the N- and C-termini

Dr. A. Koeppel, Dr. N. Stehling, Dr. C. Rodenburg, Dr. C. Holland
Department of Materials Science and Engineering
University of Sheffield
Mappin Street, Sheffield S1 3JD, United Kingdom
E-mail: christopher.holland@sheffield.ac.uk
Dr. A. Koeppel
SKZ – German Plastics Center
Friedrich-Bergius-Ring 22, 97076 Wuerzburg, Germany
Dr. N. Stehling
Codeshare Software GmbH
Moosbergstrasse 42, 64285 Darmstadt, Germany

The ORCID identification number(s) for the author(s) of this article can be found under https://doi.org/10.1002/adfm.202103295.

**ADVANCED
SCIENCE NEWS**
www.advancedsciencenews.com

**ADVANCED
FUNCTIONAL
MATERIALS**
www.afm-journal.de

interacting and interlocking.[17,26,28] Additionally, a more significant shift in pH induces an increase in β-sheet content and subsequent protein denaturation.[6,11,23,27,29]

Whilst pH appears to alter silk protein structure, the primary energetic input for silk fiber formation is flow.[30] Although silk's response to shear has been intensively studied for over 15 years,[13,27,31–33] only recently have we been able to test how silk proteins behave under extensional flow.[15] Such new insights are important, as extensional flow is by far the dominant flow field in fiber spinning and is much more efficient at aligning molecules,[34] which may facilitate hierarchical structure development.[35] However, to directly counter this hypothesis, we have recently reported that under extensional flow, native silk proteins could only form fibers at low extension rates due to dehydration, not the structural conversion typically observed during natural silk spinning.[15,36]

This per se is not necessarily a contradiction, as mentioned above prior to extensional flow silkworms and spiders condition the silk proteins by changing the pH along the gland. Therefore, we propose to further understand structure formation in naturally spun silk, it is necessary to study the interplay of pH change and extensional flow as controlled energy inputs during fiber processing.

2. Results and Discussion

Upon exposing silk proteins (obtained from fifth instar *Bombyx mori* silkworms) to acidic vapor during extensional flow, the feedstock viscosity (here indicated by the extensional stress) increases (**Figure 1**a), supporting previous observations in shear experiments.[27] This increase in viscosity is dependent on the concentration of the acid and was not observed in the absence of acidic vapor, under basic vapor exposure, or if the sample was exposed to the acidic vapor for too long (>15 s, Figure 1a and inset Figure S1, Supporting Information), as this resulted in complete gelation of the proteins.

The resulting fibers spun in vapor from a 17.5 м acetic acid solution reveal a significantly improved strength and elasticity (Figure 1b and Table S1, Supporting Information), alongside a concurrent development of structural features. Using polarized light microscopy (Figure 1c) and Fourier transform infrared (FTIR) spectroscopy, an increase in molecular alignment and a reduction in the amount of disorder in the pH-activated feedstock fibers was observed, matching that of a naturally spun silk (Figure 1d,e and Figure S2, Supporting Information).

Whilst pH activation appears necessary, to test sufficiency, that is, that structural features in silk can be formed solely by lowering the pH, we exposed a thin hand-drawn protein filament laid upon an FTIR-attenuated total reflection (ATR) crystal to acidic vapor without stretching (Figure 1f, inset image). Even after 60 s of vapor exposure, the FTIR spectra do not indicate any structural changes (Figure 1f). In a second experiment, a protein filament was exposed to acidic vapor for 10 s and then stretched with tweezers and placed onto the ATR crystal. This pH-activated, extended, sample displayed an amide I peak shift from 1641 to 1625 cm^{-1}, confirming that only through the combination of protein

acidification followed by an extensional flow can structure formation occur.

By means of an explanation, it has been shown before that a drop in pH initiates two pathways that prepare *B. mori* silk proteins for flow-induced fiber formation. In contrast to spider silk where the pH response involves conserved acidic residues, there are 19 acidic residues in fibroin that contribute toward the pH-regulated assembly. First, at a pH around 6, the fibroin N-terminal domains undergo dimerization,[26] increasing the effective molecular weight which manifests as an increase in feedstock stiffness (modulus and relaxation time), and permits a more efficient uptake of a subsequently applied mechanical stress.[26,27]
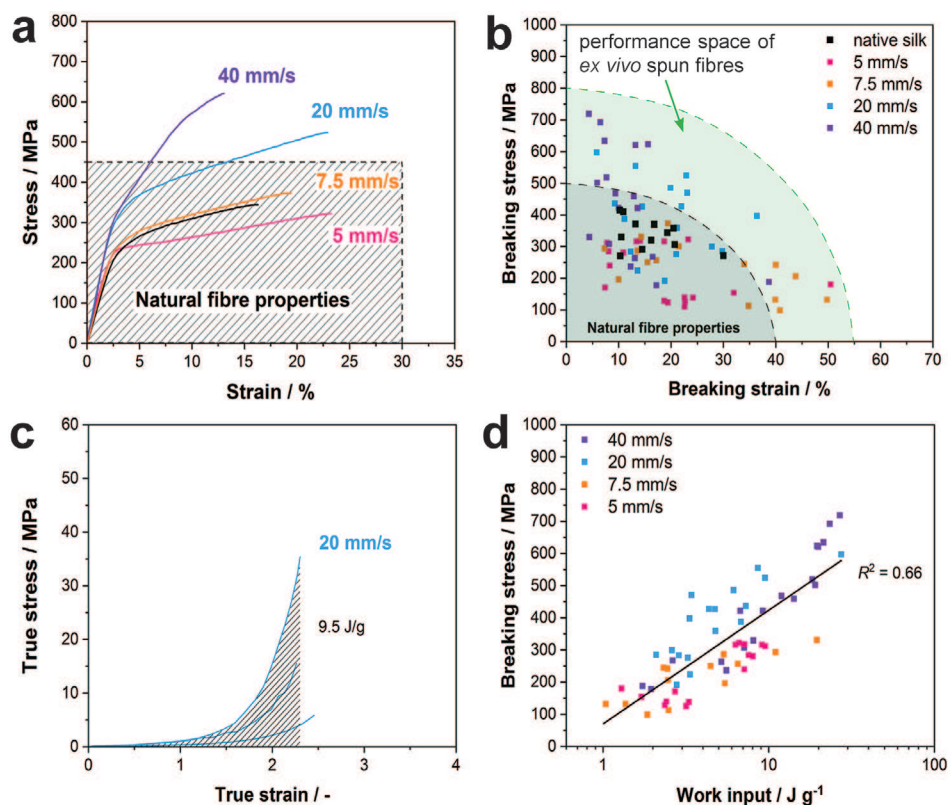
Second, a further drop in pH close to the silk protein fibroins' isoelectric point of 4.2, reduces the negative repulsive forces of neighboring chains by protonation of charged amino acid groups.[37] This allows chains to come closer together during flow, increasing alignment and subsequent hydrophobic interactions and reducing the stability of the protein, making it more susceptible to denature. Once entangled and destabilized, a subsequent extensional flow field, in excess of that which can be dissipated through relaxation of the now-gelled protein network, provides the mechanical stress input necessary to drive protein denaturation, ultimately leading to the formation of intra- and intermolecular β-sheets and a molecularly oriented, solid fiber.[26,27]

Building upon these observations and theory, using just pH activation and extension, we were able to spin silk fibers ex vivo without a specialized spinning device, chemical fixation, or post draw.[4] To replicate the conditions within the silk gland ex vivo we adjusted the diameter of the silk filament to around 50–100 µm prior to vapor exposure. Spinning using extension rates akin to natural spinning speeds (5 and 7.5 mm s^{-1}), resulted in fibers that perform like natural silkworm silk. At higher speeds (20 and 40 mm s^{-1}), fiber strength is significantly improved, supporting previous forced reeling observations (**Figure 2**a).[38] Of particular note is that in a departure from many other artificially spun silks, the shape of the stress-strain curves produced by this study also closely resemble that of the natural fiber, implying that the stress dissipation mechanisms (yield and work hardening) are similar which is most likely due to the development of comparable structural hierarchies during spinning.[4,39] Finally, the strongest ex vivo spun fiber had a breaking strength of 719.2 MPa, which is two times stronger than natural *B. mori* silk and the strongest as spun silk fiber reported to date.[4,40] We have repeated the same experiment with reconstituted and a range of recombinant silk proteins and found that these protein feedstocks cannot be spun into fibers via pH activation and subsequent extensional stretching (data not shown), an observation supported by recent studies[41] which highlight the need for additional post-processing of fibers. Possible reasons in our system could be the lower molecular weight of recombinant/reconstituted proteins as well as their insensitivity towards a drop in pH (although some recombinant systems are now becoming more pH).[42]

Despite impressive individual fiber performance, collectively the mechanical properties of ex vivo spun fibers appear to display a significant degree of variation (Figure 2b and Figure S3, Supporting Information). Explanations for such variation seen
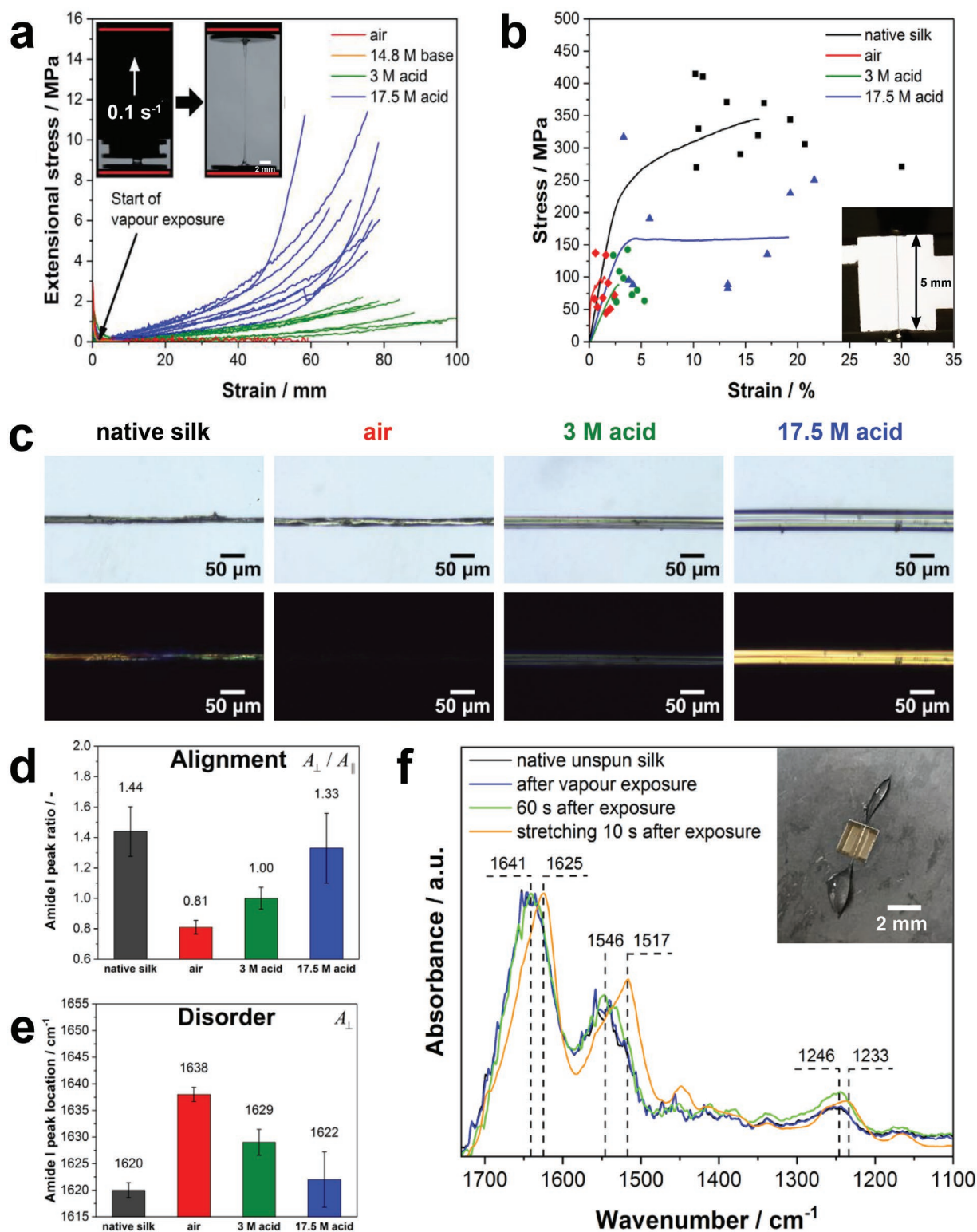
Figure 1. Mechanical and structural characterization of fibers created in air and acidic vapor at a constant strain rate of 0.1 s^{-1} a) Extensional stress of silk proteins after exposure to acidic/basic vapor. b) Mechanical properties of fibers stretched in air and vapor from different acetic acid solutions compared to native silkworm silk. c) Polarized optical microscopy images reveal orientation in silk fibers when stretched in an acidic environment. d) The analysis of the Amide I peak ratio (A$_\perp$/A$_\parallel$) provides a qualitative measure of the molecular alignment in the fibres confirming the results from polarized microscopy. e) The amount of disorder in the fibres can be analysed by the amide I peak location. A higher wavenumber indicates a lower hydrogen bonding density and therefore a higher amount of disorder. f) FTIR spectra of a thin filament of native silk proteins (see inset picture) before and after exposure to vapor from a 17.5 M acetic acid solution. Structural development in the fibers can only be observed after stretching.

ADVANCED
SCIENCE NEWS
www.advancedsciencenews.com

ADVANCED
FUNCTIONAL
MATERIALS
www.afm-journal.de

Figure 2. a) Stress/strain curves of ex vivo spun silk fibers with the best combination of strength and toughness compared to the natural fiber property region of *B. mori* silk. b) Breaking stress/strain points of all spun fibers at different extension speeds. The green area indicates a performance space of properties that can be achieved with ex vivo spun fibers depending on protein gelation and extension speed. The only variable that is actively controlled during this experiment is the spinning rate. However, the amount of acid absorbed by the proteins is different and can only be measured indirectly by analysing the stretching curve of each fiber. c) Stretching curves of three fibers that were spun at 20 mm s^{-1}. After normalising each curve to the fiber diameter, the work input can be calculated by integration (area under the curve). The curve with the highest work input is from proteins that were gelled to a higher degree by absorbing more acidic vapor compared to the other two curves. d) Breaking stress plotted against work input required for fiber formation. The work input is a qualitative measure of the degree of protein gelation prior to spinning and shows that the mechanical properties of silk fiber are not only dependent on spinning speed but also protein gelation prior to spinning.

could be due to differences between the feedstocks extracted from individual worms, or an unstable fiber drawing process.[21,32,43] However comparing our results to Figure 1, we propose that the primary cause for variability in the mechanical properties is related to the different amounts of acid vapor absorbed by the feedstock. The pH-induced protein gelation prior to spinning increases viscosity and enables the feedstock to absorb and respond to a greater amount of mechanical stress input during spinning (as denoted by the steeper curves in Figure 2c). Linking this hypothesis to fiber properties, previous work has shown that silk feedstocks require a critical shear stress threshold to be surpassed[31] and more recently a certain degree of mechanical work[44] to solidify. Upon calculating the work required for feedstock solidification, we found it centered around (7.48 ± 6.57 J g^{-1}), which is similar to recent DSC (1.78 ± 0.25 J g^{-1})[45] and shear rheology (2.75 ± 1.37 J g^{-1})[44] studies.[44,45]

Moving beyond an average and to verify pH as a source of fiber variation, we compared the work input to form a fiber, as defined by the integral of feedstock stretching stress (linked to acidification, Figure 1a), to its breaking stress (Figure 2d) and found a clear relationship between the two. The correlation

between breaking stress against work input for each individual fiber indicates that the degree of gelation prior to processing affects fiber performance and by adjusting the feedstock pH as well as the spinning speed, fiber properties can be tuned to be very strong and stiff (high work input) or weaker but more extensible (low work input) (Figure 2d).

However, the use of a cumulative work input parameter has limitations; as it does not account for the time period in which the work was applied which speaks towards efficiency. **Figure 3** displays the influence of the rate of work input (work input divided by total extension time, Figure 3a) during processing and the resulting fiber's structural and mechanical properties.

In general, fiber mechanical and structural properties improve with the rate of work input (Figure 3a,b) with our results suggesting that a rate of work input of 2 J/(g s)$^{-1}$ is required to spin fibers with properties similar to native *B. mori* silk. By comparison, fibers spun with a low rate of work input (<0.3 J (g s)$^{-1}$) tend to be more disordered and less aligned as determined by FTIR (Figure 3b) and polarized light measurements (figure 3c) but also possess a skin-core structure according to low-voltage scanning electron microscope (SEM) image of the fracture surface of an uncoated sample

2103295 (4 of 8)
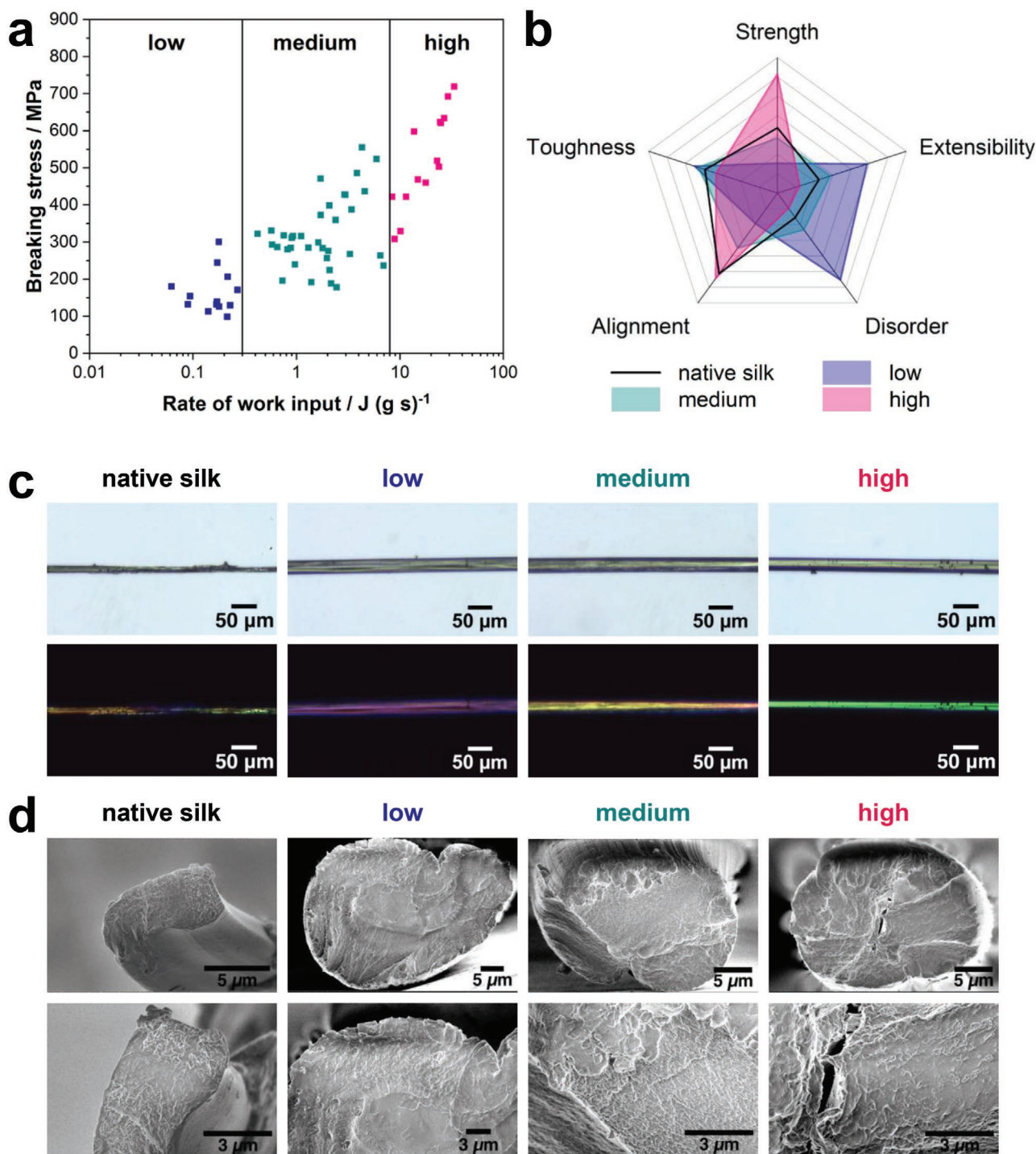
Figure 3. a) Breaking stress plotted against the rate of work input which is separated into low (<0.3 J (g s)$^{-1}$), medium (0.3 to 8 J (g s)$^{-1}$), and high (>8 J (g s)$^{-1}$). b) Mechanical and structural properties of fibers spun with low, medium, and high rates of work inputs. c) Polarized light micrographs of native silk as well as silk fibers spun with a low, medium, and high rate of work input. d) SEM micrographs of the fracture surface of native silk (one single brin is shown), as well as our silk fibers, spun with a low, medium, and high rate of work input. Note the skin-core appearance of the micrographs marked low indicating a non-uniform distribution of stress due to partial acid vapor ingress, the similarity of the features between native silk and fibers marked medium, and the sharp, clear, brittle fracture lines of high indicating more ordered structures present.

(Figure 3d). The skin-core fracture pattern confirms our hypothesis that fibers spun with a low rate of work input do so as they have taken up less acidic vapor and only the outer portion of the fiber has gelled, resulting in a more disordered fiber. The gelled regions on the outside of the fiber show a higher crystallinity that deflects the propagating crack and therefore lead to a

rougher surface. In contrast, the core of the fiber has a smooth breaking pattern which is characteristic of plastic deformation in amorphous regions. Together our structural measurements spanning the nano-to-micro scales could explain these fiber's high extensibility and toughness but low strength, agreeing with recent tensegrity modeling of silk.[46]

Feedstocks subjected to a medium rate of work input (0.3 to 8 J (g s)$^{-1}$) exhibit features akin to a native *B. mori* silk, displaying similar internal morphology and fracture surfaces under SEM (Figure 3d), degree of alignment under polarized light and FTIR (Figure 3c,b) and similar degrees of molecular disorder (Figure 3b). The fibers show a uniform fracture surface with a crack deflection at crystalline regions combined with plastic deformation in the amorphous regions. Combined this indicates that the mechanical stress applied during processing may be sufficient to align the proteins parallel to the flow direction, but insufficient to generate complete protein denaturation and ordered β-sheet conversion. In the last case, under a high rate of work input (>8 J (g s)$^{-1}$), fiber strength increases whilst the breaking strain and toughness decrease. The fracture surface is much rougher indicating much more pronounced crack deflection at the crystalline regions. Plastic deformation is much less obvious due to a rather brittle fracture. This we explain by an increase in the amount of molecular order and multiscale alignment which increases strength, but at the cost of extensibility as the amount of amorphous disordered regions responsible are reduced (Figure 3).[47]

3. Conclusion

To conclude, this study draws clear links between processing and performance in native silk proteins through two key variables, pH activation followed by extensional flow, tying both together through the concept of rate of work input. From a scientific perspective, the results presented have supported and validated previous observations and simulations surrounding hierarchical structure development in silk which in the future may facilitate new insights into silk evolution (i.e., the interaction between animal behavior and physiology). From an engineering perspective, we have successfully spun fibers without the need for complex spinning devices, chemical fixation, or post draw, with properties that meet and exceed natural *B. mori* silk, including ones that are the strongest and toughest reported to date. Our quantification of the energy efficiency of silk self-assembly provides not only important insights into how nature processes materials, but it also serves as a benchmark for future bioinspired efforts to spin artificial silks with an eye to not only recreating high-performance fibers, but to do so in an energy-conscious manner.

4. Experimental Section

Native Silk Preparation: Native silk proteins were obtained by dissecting fifth instar *B. mori* silkworms. The silk glands were extracted and transferred into distilled water where the epithelium was removed. For the experiments, only proteins from the posterior part of the middle section were used as they are predominantly free of sericin.[48]

Stretching Native Silk Proteins in Different Vapor Environments: Native silk proteins were stretched at an extension rate of 0.1 s^{-1} on the filament stretching setup used in the previous study.[15] Starting from a plate separation of 5 mm (filament diameter ≈ 100 μm), the proteins were exposed to acidic or basic vapor which was created by bringing a 2 cm x 2 cm tissue paper soaked with 40 μL of either a 3 M, 17.5 M acetic acid, or a 14.8 M ammonium hydroxide solution close to the filament for 10 s. For the experiments at constant spinning speed, the upper plate of the tensile tester was manually lifted to reduce the filament diameter to around 50 to 100 μm after the silk proteins were loaded. This was done to recreate the conditions of the natural spinning process where the pH of the protein drops inside the spinning duct (diameter 50 to 100 μm) prior to spinning. The proteins were then exposed to vapor from a 17.5 M acetic acid solution for 10 s before the stretching commenced. Fiber spinning was performed at 5, 7.5, 20, and 40 mm s^{-1}.

Polarized Optical Microscopy: The molecular alignment of the fibers was analyzed by polarized light microscopy (Diaphot-TMD inverted microscope, Nikon Corp., Japan). The fibers were oriented in a 45° angle to the crossed polarizers and images were taken with a Moticam 2500 microscope camera (Motic Electric Group Co., Ltd, China).

FTIR Measurements: FTIR measurements on single fibers were performed in ATR mode on a Nicolet 380 spectrometer (Thermo Scientific, USA). A polarizer with a ZnSe holographic wire grid (Thorlabs, USA) was used to polarize the electric field of the infrared beam perpendicular to the plane of incidence (s-polarized). Parallel and perpendicular spectra (A$_\perp$ and A$_\parallel$) were collected for each fiber from 800 to 4000 cm^{-1} at a resolution of 4 cm^{-1} by averaging over 128 scans. A baseline correction was applied by subtracting the offset value at 1730 cm^{-1} and afterwards both spectra were normalized to the intensity at 1335 cm^{-1} which was shown to be independent of orientation.[49] Both spectra were then normalized again to the amide I peak of the spectra to account for the amount of sample measured and therefore allow a comparison between different fibers. The protein chain alignment was analyzed by the ratio of the amide I peak intensities (A$_\perp$/A$_\parallel$) and the amide I peak location in the A$_\perp$ spectra revealed information about the amount of order within the fibers.

Tensile Testing: Mechanical testing was performed on a Zwick Z0.5 testing machine (Zwick GmbH & Co. KG, Germany) with a 5 N load cell at standard lab conditions (23 ± 1 °C, 50 ± 5% RH). The gauge length was set to 5 mm and tests were performed at a strain rate of 2 mm min^{-1}. The fiber diameter was determined as the average of at least 15 different measurements along the fiber axis from micrographs taken with a Diaphot-TMD inverted microscope (Nikon Corp., Japan).

Scanning Electron Microscopy: The tensile fractured fibers were prepared for SEM imaging by applying the fibers to an SEM sample holder using copper adhesive tape. The sample stage was tilted to view the tensile fractured end of the fiber top-down. SEM imaging was performed on a Nova NanoSEM450 (Thermo Fisher Scientific). The fibers were imaged uncoated at a primary beam voltage of 1 kV, 16 pA beam current, and working distances of 3–5 mm, using the through-lens secondary electron detector in immersion mode with a suction tube voltage of 250 V. Vacuum pressures were kept below 3 × 10^{-5} mbar. Image grey levels were digitally adjusted to enhance contrast.

Supporting Information

Supporting Information is available from the Wiley Online Library or from the author.

Acknowledgements

2103295 (6 of 8)

work are adapted from Andreas Koeppel's Ph.D. thesis which is available from https://etheses.whiterose.ac.uk/ under a Creative Commons Attribution Non-commercial No Derivatives (UK), in this work copyright permission has been granted by the University of Sheffield to reproduce those sections.

Conflict of Interest

The authors declare no conflict of interest.

Data Availability Statement

The data that support the findings of this study are openly available in the University of Sheffield's Online Research Data Archive (ORDA) repository http://doi.org/10.15131/shef.data.14573676.

Keywords

[1] a) F. Vollrath, D. Porter, *Polymer* **2009**, *50*, 5623; b) T. D. Sutherland, J. H. Young, S. Weisman, C. Y. Hayashi, D. J. Merritt, *Annu. Rev. Entomol.* **2010**, *55*, 171; c) C. L. Craig, *Annu. Rev. Entomol.* **1997**, *42*, 231; d) T. Asakura, D. Kaplan, *Encycl. Agric. Sci.* **1994**, *4*, 1; e) H. Heslot, *Biochimie* **1998**, *80*, 19; f) F. Vollrath, D. Porter, C. Holland, *Soft Matter* **2011**, *7*, 9595; g) J. M. Gosline, P. A. Guerette, C. S. Ortlepp, K. N. Savage, *J. Exp. Biol.* **1999**, *202*, 3295; h) A. R. Bunsell, *Handbook of tensile properties of textile and technical fibers*, Woodhead Publishing, Cambridge, UK **2009**.

[2] S. Keten, Z. Xu, B. Ihle, M. J. Buehler, *Nat. Mater.* **2010**, *9*, 359.

[3] J. L. Yarger, B. R. Cherry, A. van der Vaart, *Nat. Rev. Mater.* **2018**, *3*, 18008.

[4] A. Koeppel, C. Holland, *ACS Biomater. Sci. Eng.* **2017**, *3*, 226.

[5] Y. Yao, B. J. Allardyce, R. Rajkhowa, D. Hegh, A. Sutti, S. Subianto, S. Gupta, S. Rana, S. Greenhill, S. Venkatesh, X. Wang, J. M. Razal, *ACS Biomater. Sci. Eng.* **2020**, *6*, 3197.

[6] C. W. P. Foo, E. Bini, J. Hensman, D. P. Knight, R. V. Lewis, D. L. Kaplan, *Appl. Phys. A* **2006**, *82*, 223.

[7] A. Ochi, K. S. Hossain, J. Magoshi, N. Nemoto, *Biomacromolecules* **2002**, *3*, 1187.

[8] L. Zhou, X. Chen, Z. Shao, Y. Huang, D. P. Knight, *J. Phys. Chem. B* **2005**, *109*, 16937.

[9] L. Zhou, X. Chen, Z. Shao, P. Zhou, D. P. Knight, F. Vollrath, *FEBS Lett.* **2003**, *554*, 337.

[10] a) L. J. Domigan, M. Andersson, K. A. Alberti, M. Chesler, Q. Xu, J. Johansson, A. Rising, D. L. Kaplan, *Insect Biochem. Mol. Biol.* **2015**, *65*, 100; b) A. Percot, P. Colomban, C. Paris, H. M. Dinh, M. Wojcieszak, B. Mauchamp, *Vib. Spectrosc.* **2014**, *73*, 79; c) F. Vollrath, D. P. Knight, X. W. Hu, *Proc. R. Soc. B* **1998**, *265*, 817.

[11] T. Asakura, K. Umemura, Y. Nakazawa, H. Hirose, J. Higham, D. Knight, *Biomacromolecules* **2007**, *8*, 175.

[12] a) J. Magoshi, Y. Magoshi, S. Nakamura, presented at ACS Symposium series number 544, USA, **1994**; b) C. Viney, *Supramol. Sci.* **1997**, *4*, 75; c) F. Vollrath, D. P. Knight, *Nature* **2001**,
410, 541; d) D. P. Knight, M. M. Knight, F. Vollrath, *Int. J. Biol. Macromol.* **2000**, *27*, 205; e) J. Sparkes, C. Holland, *Nat. Commun.* **2017**, *8*, 594.

[13] C. Holland, A. E. Terry, D. Porter, F. Vollrath, *Nat. Mater.* **2006**, *5*, 870.

[14] a) C. Holland, F. Vollrath, A. J. Ryan, O. O. Mykhaylyk, *Adv. Mater.* **2012**, *24*, 105; b) X. Wang, Y. Li, Q. Liu, Q. Chen, Q. Xia, P. Zhao, *Biochim. Biophys. Acta, Gen. Subj.* **2016**, *1861*, 567.

[15] A. Koeppel, P. R. Laity, C. Holland, *Soft Matter* **2018**, *14*, 8838.

[16] C. Dicko, F. Vollrath, J. M. Kenney, *Biomacromolecules* **2004**, *5*, 704.

[17] G. Askarieh, M. Hedhammar, K. Nordling, A. Saenz, C. Casals, A. Rising, J. Johansson, S. D. Knight, *Nature* **2010**, *465*, 236.

[18] a) J. Zhong, Y. Liu, J. Ren, Y. Tang, Z. Qi, X. Zhou, X. Chen, Z. Shao, M. Chen, D. L. Kaplan, S. Ling, *ACS Biomater. Sci. Eng.* **2019**, *5*, 3161; b) M. Saric, T. Scheibel, *Curr. Opin. Biotechnol.* **2019**, *60*, 213.

[19] M. Andersson, J. Johansson, A. Rising, *Int. J. Mol. Sci.* **2016**, *17*, 1290.

[20] A. D. Malay, T. Suzuki, T. Katashima, N. Kono, K. Arakawa, K. Numata, *Sci. Adv.* **2020**, *6*, eabb6030.

[21] P. R. Laity, E. Baldwin, C. Holland, *Macromol. Biosci.* **2019**, *19*, 1800188.

[22] A. Koeppel, P. R. Laity, C. Holland, *Acta Biomater.* **2020**, *117*, 204.

[23] C. Dicko, J. M. Kenney, D. Knight, F. Vollrath, *Biochemistry* **2004**, *43*, 14080.

[24] a) C. Schaefer, P. R. Laity, C. Holland, T. C. B. McLeish, *Macromolecules* **2020**, *53*, 2669; b) C. Schaefer, P. R. Laity, C. Holland, T. C. B. McLeish, *Molecules* **2021**, *26*, 1663.

[25] a) P. Chen, H. S. Kim, C. Y. Park, H. S. Kim, I. J. Chin, H. J. Jin, *Macromol. Res.* **2008**, *16*, 539; b) S. Rammensee, U. Slotta, T. Scheibel, A. R. Bausch, *Proc. Natl. Acad. Sci. U. S. A.* **2008**, *105*, 6590; c) S. Schwarze, F. U. Zwettler, C. M. Johnson, H. Neuweiler, *Nat. Commun.* **2013**, *4*, 2815; d) F. Hagn, C. Thamm, T. Scheibel, H. Kessler, *Angew. Chem., Int. Ed.* **2011**, *50*, 310.

[26] Y.-X. He, N.-N. Zhang, W.-F. Li, N. Jia, B.-Y. Chen, K. Zhou, J. Zhang, Y. Chen, C.-Z. Zhou, *J. Mol. Biol.* **2012**, *418*, 197.

[27] A. E. Terry, D. P. Knight, D. Porter, F. Vollrath, *Biomacromolecules* **2004**, *5*, 768.

[28] a) A. Rising, J. Johansson, *Nat. Chem. Biol.* **2015**, *11*, 309; b) M. Strickland, V. Tudorica, M. Řezáč, N. R. Thomas, S. L. Goodacre, *Heredity* **2018**, *120*, 574.

[29] X. H. Zong, P. Zhou, Z. Z. Shao, S. M. Chen, X. Chen, B. W. Hu, F. Deng, W. H. Yao, *Biochemistry* **2004**, *43*, 11932.

[30] J. Sparkes, C. Holland, *Macromol. Biosci.* **2019**, *19*, 1800229.

[31] P. Laity, C. Holland, *Int. J. Mol. Sci.* **2016**, *17*, 1812.

[32] P. R. Laity, S. E. Gilks, C. Holland, *Polymer* **2015**, *67*, 28.

[33] a) P. R. Laity, C. Holland, *Eur. Polym. J.* **2017**, *87*, 519; b) P. R. Laity, C. Holland, *Biomacromolecules* **2016**, *17*, 2662; c) N. Kojic, J. Bico, C. Clasen, G. H. McKinley, *J. Exp. Biol.* **2006**, *209*, 4355.

[34] a) M. Sentmanat, O. Delgadillo-Velázquez, S. G. Hatzikiriakos, *Rheol. Acta* **2010**, *49*, 931; b) M. Trebbin, D. Steinhauser, J. Perlich, A. Buffet, S. V. Roth, W. Zimmermann, J. Thiele, S. Förster, *Proc. Natl. Acad. Sci. U. S. A.* **2013**, *110*, 6706.

[35] a) M. R. Khan Md, H. Morikawa, Y. Gotoh, M. Miura, Z. Ming, Y. Sato, M. Iwasa, *Int. J. Biol. Macromol.* **2008**, *42*, 264; b) Q. Wan, K. J. Abrams, R. C. Masters, A. C. S. Talari, I. U. Rehman, F. Claeyssens, C. Holland, C. Rodenburg, *Adv. Mater.* **2017**, *29*, 1703510.

[36] D. Ebrahimi, O. Tokareva, N. G. Rim, J. Y. Wong, D. L. Kaplan, M. J. Buehler, *ACS Biomater. Sci. Eng.* **2015**, *1*, 864.

[37] C.-Z. Zhou, F. Confalonieri, N. Medina, Y. Zivanovic, C. Esnault, T. Yang, M. Jacquet, J. Janin, M. Duguet, R. Perasso, Z.-G. Li, *Nucleic Acids Res.* **2000**, *28*, 2413.

[38] a) B. Mortimer, C. Holland, F. Vollrath, *Biomacromolecules* **2013**, *14*, 3653; b) Z. Shao, F. Vollrath, *Nature* **2002**, *418*, 741.

[39] a) J. Guan, F. Vollrath, D. Porter, in *6th BACSA International Conference: Building value Chains in Sericulture*, Padua, Italy **2013**; b) J. Guan, D. Porter, F. Vollrath, *Polymer* **2012**, *53*, 2717;

**ADVANCED
SCIENCE NEWS**

www.advancedsciencenews.com

**ADVANCED
FUNCTIONAL
MATERIALS**

www.afm-journal.de

c) J. Guan, D. Porter, F. Vollrath, *Biomacromolecules* **2013**, *14*, 930; d) B. Mortimer, D. R. Drodge, K. I. Dragnevski, C. R. Siviour, C. Holland, *J. Mater. Sci.* **2013**, *48*, 5055; e) B. Mortimer, J. Guan, C. Holland, D. Porter, F. Vollrath, *Acta Biomater.* **2015**, *11*, 247.

[40] M. Frydrych, A. Greenhalgh, F. Vollrath, *Sci. Rep.* **2019**, *9*, 15428.

[41] a) W. Finnigan, A. D. Roberts, C. Ligorio, N. S. Scrutton, R. Breitling, J. J. Blaker, E. Takano, *Sci. Rep.* **2020**, *10*, 10671; b) G. Greco, J. Francis, T. Arndt, B. Schmuck, F. G. Bäcklund, A. Barth, J. Johansson, N. M. Pugno, A. Rising, *Molecules* **2020**, *25*, 3248; c) N. Gonska, P. A. López, P. Lozano-Picazo, M. Thorpe, G. V. Guinea, J. Johansson, A. Barth, J. Pérez-Rigueiro, A. Rising, *Biomacromolecules* **2020**, *21*, 2116.

[42] T. Arndt, P. R. Laity, J. Johansson, C. Holland, A. Rising, *ACS Biomater. Sci. Eng.* **2021**, *7*, 462.

[43] S. W. Ha, A. E. Tonelli, S. M. Hudson, *Biomacromolecules* **2005**, *6*, 1722.

[44] J. Sparkes, C. Holland, *Macromol. Biosci.* **2018**, *19*, 1800229.

[45] C. Holland, N. Hawkins, M. Frydrych, P. Laity, D. Porter, F. Vollrath, *Macromol. Biosci.* **2019**, *19*, 1800228.

[46] F. Fraternali, N. Stehling, A. Amendola, B. A. Tiban Anrango, C. Holland, C. Rodenburg, *Nanomaterials* **2020**, *10*, 1510.

[47] A. Nova, S. Keten, N. M. Pugno, A. Redaelli, M. J. Buehler, *Nano Lett.* **2010**, *10*, 2626.

[48] a) H. Akai, *Experientia* **1983**, *39*, 443; b) J. Machida, *Proc. Imp. Acad.* **1926**, *2*, 421.

[49] M. Boulet-Audet, T. Lefèvre, T. Buffeteau, M. Pézolet, *Appl. Spectrosc.* **2008**, *62*, 956.